PERGAMON

Continental Shelf Research 21 (2001) 1219–1236

CONTINENTAL SHELF RESEARCH

www.elsevier.com/locate/csr

Mesoscale variability in the boundary currents of the Alaska Gyre

Stephen R. Okkonen*, Gregg A. Jacobs, E. Joseph Metzger, Harley E. Hurlburt, Jay F. Shriver

Ocean Dynamics and Prediction Branch, Naval Research Laboratory, Stennis Space Center, MS 39529, USA

Received 13 December 1999; accepted 29 June 2000

Abstract

Measurements of sea-surface height anomalies acquired during the GEOSAT, ERS-1, and TOPEX altimeter missions show that the boundary currents of the Alaska gyre exhibit interannual variability with respect to the occurrence, size, and propagation of mesoscale, eddy-like features. Observations and model results suggest that eddies are generated in the Alaska Current during years in which the wind forcing in the eastern Gulf of Alaska promotes strong downwelling along the British Columbia–Alaska coast. Wind forcing conditions that support eddy formation and intensification often occur in years that coincide with El Niño–Southern Oscillation events. Eddy variability is significantly more deterministic in the Alaska Current than in the Alaskan Stream.

Keywords: Eastern boundary current; Western boundary current; Mesoscale eddies; Modelling; Radar altimetry

1. Introduction

The subpolar Alaska gyre resides in the atmospherically energetic northeastern corner of the North Pacific Ocean. Its mean circulation is cyclonic and is circumscribed by the eastward-flowing Subarctic Current, the broad, poleward-flowing Alaska Current, and the strong, southwestward-flowing Alaskan Stream (Fig. 1). The Alaska Current and Alaskan Stream are, respectively, the eastern and western boundary currents of the gyre. Despite an order of magnitude change in the seasonal wind forcing over the gulf (Reed et al., 1980), weak annual signals have been generally ascribed to the baroclinic transports of the Alaska Current (Tabata, 1991) and the Alaskan Stream (Reed et al., 1980). However, significant interannual transport variability has been reported for the Alaska Current (Tabata, 1991) and can be inferred for the Alaskan Stream (e.g.

*Corresponding author.

0278-4343/01/$ - see front matter
PII: S0278-4343(00)00085-6

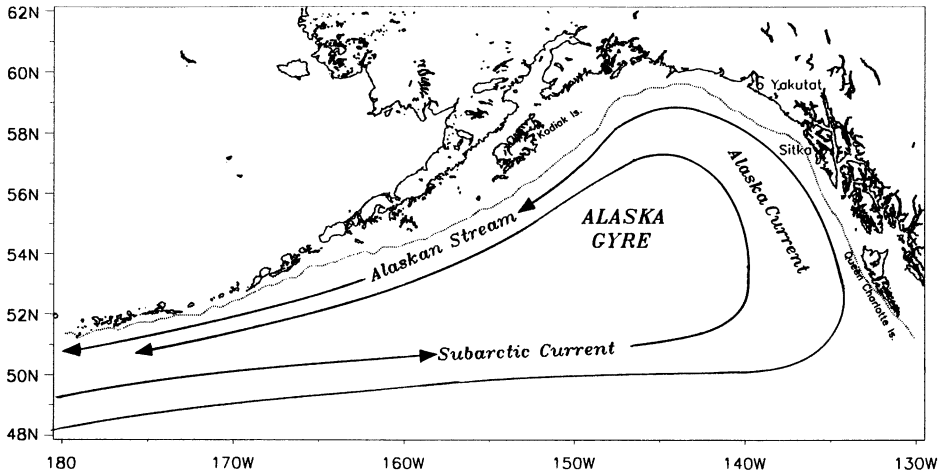

Fig. 1. Currents and place names for the Gulf of Alaska region. The 1000 m isobath is shown as a dotted line.

Favorite, 1974; Reed, 1984; Musgrave et al., 1992; Reed and Stabeno, 1994). Reed (1984) and Tabata (1991) have attributed this variability to interannual period variations in the regional wind forcing. These interannual variations have been associated with El Niño/Southern Oscillation (ENSO) events (Emery and Hamilton, 1985; Johnson and O'Brien, 1990), as have interannual variations in sea-level height along the coast of the Gulf of Alaska (Chelton and Davis, 1982) and the generation of interannual period baroclinic Rossby waves in the region (White and Tabata, 1987; Jacobs et al., 1994). Lagerloef (1995) also identified interdecadal variability in Alaska gyre circulation, which he attributed to long-period variations in the regional wind forcing. An excellent review of research literature on oceanic and atmospheric variability in the northeast Pacific Ocean, and its relationship to ENSO events, was provided by Mysak (1986).

In contrast to the gyre-scale circulation and its variability, the occurrence and variability of mesoscale features in the boundary currents of the Alaska gyre have not been as well studied. A notable exception is the Sitka eddy (Tabata, 1982) which has been frequently observed, often in the company of other eddies, within the Alaska Current. Willmott and Mysak (1980) proposed that reflection of atmospherically forced planetary waves in the northeast Gulf of Alaska generates these eddies. Swaters and Mysak (1985) later proposed that the interaction between the Alaska Current and the underlying topography contributes to the generation of the Sitka eddy. They also noted that years in which the Sitka eddy was observed to occur were also years in which the winter atmospheric circulation over the gulf was anomalously strong. Cummins (1989) expanded an earlier numerical study of circulation in the Alaska gyre (Cummins and Mysak, 1988) to investigate the effects of topography and seasonal wind forcing on the regional circulation. Results from his three-layer, quasi-geostrophic model indicated that the inclusion of topography significantly reduced both the effects of seasonal forcing on regional circulation and the amplitudes of mesoscale eddies in comparison to circulation conditions evident in flat-bottom simulations. More recently, Thomson and Gower (1998) reported on a well-defined chain of anticyclonic eddies residing along the eastern margin of the Gulf of Alaska. They suggested that the generation of these eddies was triggered by an abrupt reversal in the prevailing poleward

winds. Melsom et al. (1999) have investigated the relationship between interannual variations in the number and strength of eddies and El Niño/La Niña events.

Elsewhere, Okkonen (1992) used GEOSAT altimeter data to monitor the shedding of a large, anticyclonic eddy from the Alaskan Stream near the central Aleutian Islands. A theoretical model predicting instability of the Alaskan Stream in the central Aleutian region, and the shedding of anticyclonic eddies, was developed by Thomson (1972). Also using altimeter data to investigate the mesoscale environment in the Alaska gyre, Gower (1989), Matthews et al. (1992), Lagerloef et al. (1993) and Crawford et al. (2000) all reported the occurrence of westward-propagating, eddy-like features. Gower (1989), in particular, identified individual westward-propagating eddies originating near Yakutat and Sitka, Alaska as well as near either end of the Queen Charlotte Islands, British Columbia, whereas Crawford et al. (2000) reported on multi-year eddies in the Alaskan Stream.

This paper presents observations of propagating, mesoscale meanders/eddies (hereafter "eddies") in the Alaska Current and Alaskan Stream. These observations are multi-year, synoptic surveys compiled from measurements of sea-surface height (SSH) anomalies acquired by the GEOSAT, ERS-1, and TOPEX satellite altimeters. Results from 1/16° global simulations by the Naval Research Laboratory Layered Ocean Model (NLOM) (Metzger et al., 1998; Hurlburt and Hogan, 2000; Shriver and Hurlburt, 2000; Tilburg et al., 2001) are also analyzed and compared to the observations to suggest mechanisms which account for the occurrence and evolution of the mesoscale eddies. A similar 1/16° Pacific Ocean model north of 20°S has been used to investigate Kuroshio region dynamics (Hurlburt et al., 1996; Hurlburt and Metzger, 1998) and Hawaiian Island region dynamics (Leonardi et al., 2001). Melsom et al. (1999) used a 1/8° version of the NLOM Pacific model in their study of eddy generation in the eastern Alaska Gyre.

2. Altimeter data

Altimeter data from the Gulf of Alaska region used in this study include observations from GEOSAT (fall 1986 to fall 1989), from ERS-1 (spring 1992 to winter 1993), and from TOPEX (fall 1992 to summer 1995). Standard corrections were applied to these data (the Grenoble tidal model, Le Provost et al. (1994), was used for the ocean tide correction) after which the temporal mean SSHs (1987–1988 for GEOSAT, 1993–1994 for TOPEX, 4/1992–12/1993 for ERS-1) were computed at each ground track point according to the method described by Leben et al. (1990) and then removed from the respective data sets to yield working data sets of SSH anomalies in the Gulf of Alaska.

For both the GEOSAT and TOPEX missions, local maxima of averaged, altimetrically measured, positive SSH displacements in the boundary current region delineated a mean corridor along which many anticyclonic eddies were observed to propagate. The location of the eddy corridor for each mission was determined as follows. A space–time average of positive SSH anomalies, $\bar{h}_x$, was computed at each location, x, along orbital ground-track segments extending ~200 km (30 points for GEOSAT data and 35 points for TOPEX data) seaward from the 1000 m isobath

$$\bar{h}_x = \frac{\sum_{t=1}^{n} \sum_{i=-2}^{2} h_{x+i,t}}{\sum_{t=l}^{n} m_t}, \tag{1}$$

where h refers to only those positive SSH anomalies $\geqslant 5$ cm (approximately the gyre-wide mean rms SSH variability), m is the number of locations between $x-2$ and $x+2$ ($0 \leqslant m \leqslant 5$) at which the height of the anomaly is greater than 5 cm during orbital repeat cycle t, and n is the number of orbital repeat cycles for the particular altimeter mission. The inshore limit of the ground-track segment was chosen to exclude measurements acquired over the continental shelf where variability associated with residual tidal errors may have remained significant. The offshore limit was chosen to include the greatest offshore excursion of the Alaskan Stream (~200 km: Musgrave et al., 1992). For most ground-track segments, the absolute maximum of $\bar{h}_x$ was selected as a point along the mean corridor. For a few ground-track segments, the location of a second local maximum of $\bar{h}_x$ was chosen as the point on the mean corridor if the location of the absolute maximum diverged significantly from a subjectively defined "smooth" corridor. Because the ERS-1 and TOPEX missions overlapped, the locations defining the eddy corridor for the ERS-1 mission were taken to be those at which the ERS-1 ground tracks crossed the TOPEX corridor. Finally, SSH anomalies along the corridors were partitioned into 1.25° longitude by 1-month bins (GEOSAT data) and 2.0° longitude by 1-month bins (ERS-1 and TOPEX data) and then averaged.

3. Observations

The eddy corridors, as determined from measurements of SSH anomalies acquired during the GEOSAT, ERS-1, and TOPEX missions, are plotted in Fig. 2. The time–longitude plot of the bin-averaged GEOSAT SSH anomalies that occur along this corridor reveals long-lived mesoscale eddies which propagate along the boundary of the gulf (Fig. 3). Eddy "A_G" (where "G" denotes the GEOSAT mission) corresponds to the large meander/eddy described by Okkonen (1992, 1996)

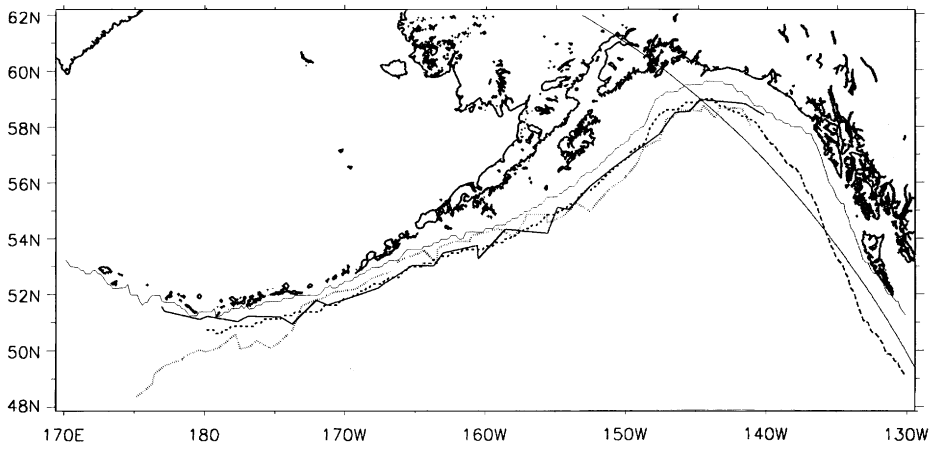

Fig. 2. The mean corridors traversed by propagating eddies in the boundary currents of the Alaska gyre during the GEOSAT mission (dotted), TOPEX mission (thick solid), and for the Naval Research Laboratory Layered Ocean Model simulations (short dash). An additional segment (long dash) delineates the region along the British Columbia–Alaska coast where the generation of model eddies was monitored. TOPEX ground-track D91 is shown as a solid line passing from northwest to southeast through the eastern Gulf of Alaska. The 1000 m isobath is shown as a thin solid line.

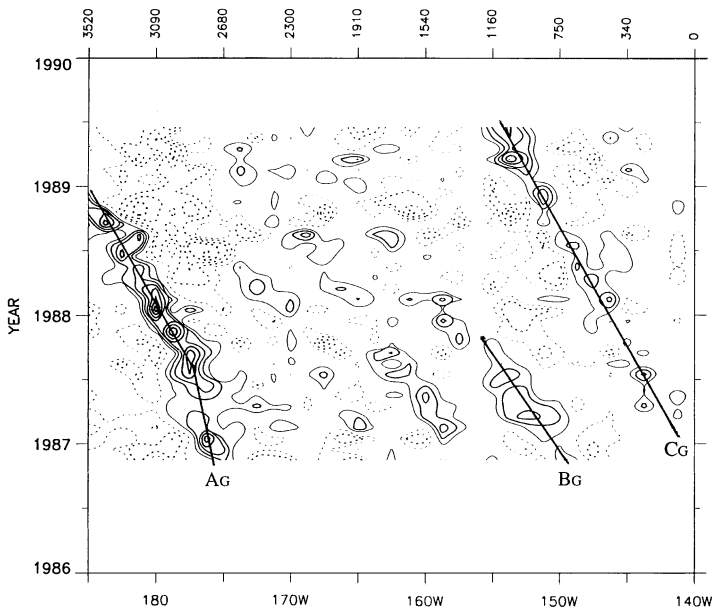

Fig. 3. Time–longitude plot of the SSH anomalies along the eddy corridor for the GEOSAT mission. The contour interval is 5 cm. Solid line contours indicate positive anomalies and dashed line contours indicate negative anomalies. The zero contours are omitted. An along-shelf distance scale (km) is provided at the top of the figure. The labeled eddies are discussed in the text.

and exhibits an along-shore phase velocity of $\sim$1.1 cm s^{-1}. Eddy "B_G" propagates southwestward along the shelf break to about 160°W at $\sim$1.9 cm s^{-1}. It also appears in contemporaneous current meter records as a flow reversal extending to a depth of at least 1100 m and, later, as a meander in drifter tracks downstream from the mooring location (Reed and Stabeno, 1989). The region between eddies "A_G" and "B_G", from $\sim$158°W to $\sim$173°W, is characterized by short-lived, small-amplitude mesoscale features. Eddy "C_G", which propagates along shore at $\sim$1.3 cm s^{-1}, corresponds to an anticyclonic eddy which Gower (1989) reported as originating near Yakutat, Alaska (59.3°N, 141.4°W) in early 1987 and which later appeared near Kodiak Island, as evidenced in hydrography and drifter tracks acquired in 1988 and 1989 (Musgrave et al., 1992). The apparent topographic signature of eddy "C_G" during 1987 is relatively weak because that portion of the corridor along which it is measured is irregular and lies somewhat to the south of that reported by Gower (1989).

Eddies formed in the Alaska Current tend to propagate away from the coast toward the interior of the Alaska gyre. Time series of SSH anomaly profiles along ascending GEOSAT orbital ground tracks nearest the British Columbia–Alaska (BC–Alaska) coastline provide a means by which to monitor the occurrence of the Yakutat, Sitka, and Queen Charlotte eddies. Matthews et al. (1992) presented these data in a time–latitude format which showed the formation of moderate-to-large eddy-like features near Yakutat and Sitka in 1987 and 1988 and near the Queen Charlotte Islands in 1987.

Fig. 4 shows the composite time–longitude plot constructed from the bin-averaged SSH anomalies measured along the eddy corridor during the ERS-1 and TOPEX missions (cf. Fig. 2).

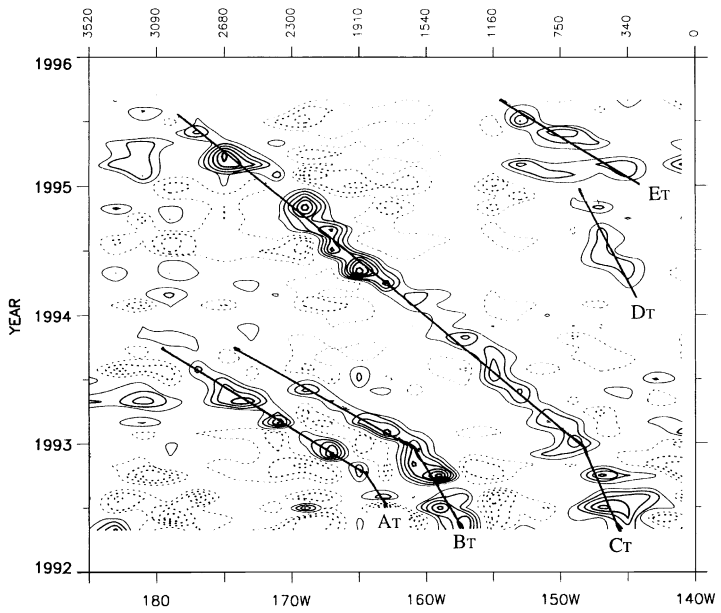

Fig. 4. Time–longitude plot of the SSH anomalies along the eddy corridor for the combined ERS-1 and TOPEX missions. The contour interval is 5 cm. Solid line contours indicate positive anomalies and dashed line contours indicate negative anomalies. The zero contours are omitted. An along-shelf distance scale (km) is provided at the top of the figure. The labeled eddies are discussed in the text.

The periods of coverage overlap for these two missions and provide a longer record of coverage than does either mission individually. Eddies "A_T" and "B_T" (where "T" denotes a meander or eddy observed during the ERS-1 and/or TOPEX missions) first appear in the altimeter data near 160°W. Their initial along-shore phase speed is $\sim 1.0\,\mathrm{cm\,s^{-1}}$. In late 1992, both anomalies apparently sped up to propagate at about $\sim 3.7\,\mathrm{cm\,s^{-1}}$. The associated period and along-shore wavelength are ~130 days (in spring 1993) and ~415 km (near 170°W), respectively. Eddy "B_T" appears as a meander in a drifter track reported by Reed and Stabeno (1994). Eddy "C_T" is remarkable in that it remains a coherent feature for three years during which it propagates over 2300 km at $\sim 2.8\,\mathrm{cm\,s^{-1}}$ from the head of the Gulf of Alaska to the central Aleutians. Anomalies "D_T" and "E_T" originate near Yakutat, Alaska in early 1994 and 1995, respectively. Anomaly "D_T" does not appear to propagate very far downstream, while there is not a sufficient number of measurements to determine the longevity of anomaly "E_T".

Although the TOPEX descending orbital ground tracks are a bit more oblique to the BC–Alaska coast than are the GEOSAT ascending ground tracks, the time series of the altimetrically derived velocity anomalies orthogonal to TOPEX orbital ground track D91 (Fig. 5) shows that Queen Charlotte eddies (~132–136°W) occur most significantly in 1995, whereas the most significant Sitka eddies (~139–141°W) occur in 1993 and 1995. The velocity anomalies are used here instead of SSH anomalies because long-wavelength signals in the SSH anomaly field obscure shorter wavelength signals.

Comparing Figs. 3 and 4, it is seen that the amplitudes of Alaskan Stream eddies observed during the GEOSAT mission are generally less than those observed during the ERS-1 and

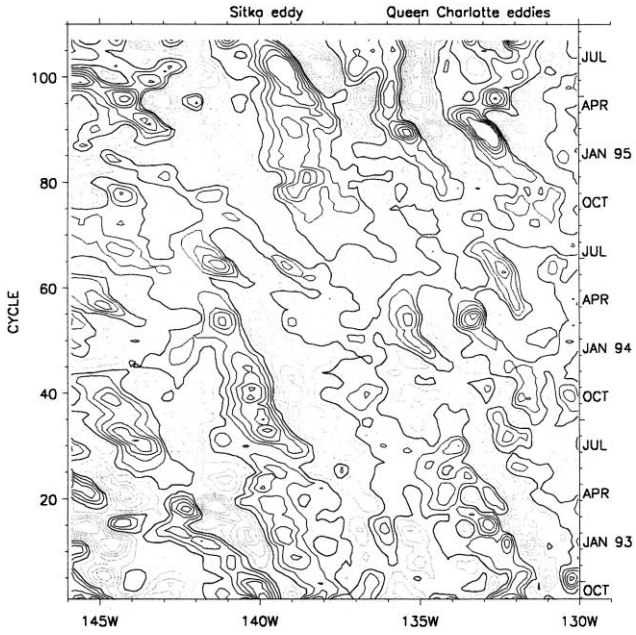

Fig. 5. Time–longitude plot of the velocity anomalies orthogonal to TOPEX descending ground-track D91. The longitudinal locations of Sitka eddy signals and Queen Charlotte signals are shown at the top of the figure. Solid line contours indicate zero and positive anomalies and dashed line contours indicate negative anomalies. The contour interval is $5\,\mathrm{cm\,s^{-1}}$.

TOPEX missions. Unfortunately, the absence of observational data for the intervening years makes it difficult to determine a cause or causes to which the disparity in amplitudes may be attributed. To address this shortcoming and to aid in the interpretation of the observational data we will make use of high-resolution numerical simulations of interdecadal circulation in the Gulf of Alaska.

4. The Naval Research Laboratory Layered Ocean Model (NLOM)

The version of the NLOM used in this study is an enhanced version (Wallcraft, 1991) of a primitive equation model whose lineage is traced to a model developed by Hurlburt and Thompson (1980). The present model has a horizontal resolution of $1/16^\circ$ in latitude and $45/512^\circ$ in longitude and a temporal sampling of model fields at 3.05-day intervals. It simulates global circulation for the years 1979–1997 (see Hurlburt and Hogan (2000) for details on the model formulation). The model has realistic bathymetry and is forced by realistic 1000 mb European Centre for Medium-Range Weather Forecasts winds (ECMWF User's Guide, 1995). The 6-hourly ECMWF reanalysis winds (Gibson et al., 1997) were used to drive the model for years prior to and including 1993, whereas 12-hourly ECMWF operational winds were used for model years 1994–1997. In order to assess the intrinsic interannual variability of the NLOM, the model was run twice. For both simulations, the model was spun up using the Hellerman and Rosenstein

(1983) wind stress climatology. After achieving statistical equilibrium, the model runs were forced with interannual ECMWF winds with the long-term mean replaced by the annual mean from Hellerman–Rosenstein. The two simulations differed only in the times at which the re-initialization with the interannual winds occurred. For both simulations, a 17-year mean (1979–1995) SSH, computed at each model grid point, was subtracted from each record of SSH at each corresponding grid point in the Gulf of Alaska. The resulting space–time matrices of model SSH anomalies were sub-sampled every third record to provide working data sets having an effective temporal sampling period of 9.15 days.

The ability of the NLOM to accurately reproduce observed SSH variability in the Gulf of Alaska is demonstrated by comparing time series of model sea level with observed sea level at various locations around the Gulf of Alaska. An example from Sitka, which is representative of other locations along the eastern boundary of the gulf, is shown in Fig. 6. The interannual variability shows a range of about 30 cm. Correlation coefficients for the time series (Table 1)

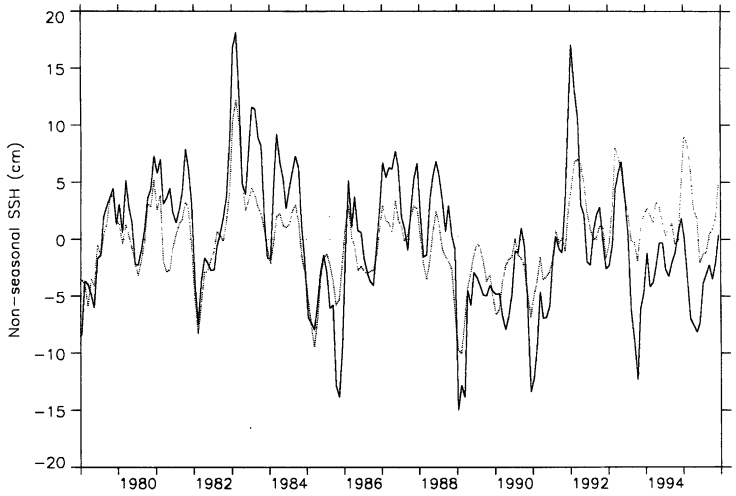

Fig. 6. Time series of monthly mean Integrated Global Ocean System Services (IGOSS) sea-level height (solid) and modeled sea-level height (dotted) at Sitka, Alaska. The data have been smoothed with a 3-month running mean.

Table 1
Correlation coefficients between observed Integrated Global Ocean Services System (IGOSS) sea-level data and NLOM sea level at various locations around the Gulf of Alaska. Both data sets have been smoothed by 30-day and 12-month running means prior to computation of the respective correlation coefficients

IGOSS station	30-day mean	12-month mean
Prince Rupert, Canada	0.68	0.93
Sitka, Alaska	0.70	0.89
Yakutat, Alaska	0.61	0.80
Seward, Alaska	0.53	0.80
Unalaska, Alaska	0.43	0.83

indicate that the model reproduces reasonably well the annual and interannual variability observed to occur in the boundary region of the gulf and therefore suggest that the model may be a useful tool to assist in the investigation of interannual, mesoscale variability in the boundary currents of the Alaska gyre.

An eddy corridor for model SSH anomalies occurring in the Alaskan Stream was set to lie at an offshore distance representative of that computed from altimeter data (~55 km, i.e. eight model grid points south of the 1000 m isobath). Upstream of the eddy corridor (east of 140°W), additional NLOM grid points near GEOSAT ascending ground track A173 were chosen to monitor the generation of model eddies in the Alaska Current along the BC–Alaska coast. At the head of the gulf, the eddy corridor and monitoring segment were adjusted to produce a smooth intersection (cf. Fig. 2). The combined eddy corridor and monitoring segment will, hereafter, be referred to as the eddy corridor, with the understanding that eddies generated along the monitoring segment propagate westward away from the BC–Alaska coast toward the interior of the gyre. For both simulations, time series of model SSH anomalies along the eddy corridor were then partitioned into 45/256° longitude by 1-month bins, averaged, and plotted in a time–longitude format (Figs. 7a and b).

Although there are differences between the model eddy fields in the Alaska Current, both simulations show that large anticyclonic eddies are generated near Yakutat (~141–144°W), Sitka (~137–139°W), and the Queen Charlotte Islands (~130–135°W) during many years. In particular, large Queen Charlotte eddies were generated in 1983, 1992, and 1995 while large amplitude Yakutat and Sitka eddies were generated in 1983, 1992, 1993, and 1995. Eddy amplitudes along the BC–Alaska coast were smallest during 1982, 1985, and 1988 through 1990. Yakutat eddies propagate downstream at ~1–2 cm s^{-1} until their topographic signatures effectively disappear between 150°W and 155°W.

While there are many years in which moderate-to-large amplitude eddies appear near Kodiak Island (~150°W), there are only a few years in which model eddies appear in the Alaskan Stream southwest of Kodiak. In the first simulation (Fig. 7a), a strong Alaskan Stream eddy is evident near 160°W in 1979 and a somewhat weaker eddy appears near 150°W. Over the next couple of years, the latter eddy propagates downstream to near 175°W. Somewhat weaker eddies appear near 160°W in 1984, 1987, and 1992. In the second simulation (Fig. 7b), Alaskan Stream eddies appear near 160°W in early 1979, late 1983 and 1992. Additionally, the occurrence of Alaskan Stream eddies in 1995 is suggested in both simulations by spatial periodicity of the SSH anomaly field between 155°W and 170°W.

The similarities and differences between the two simulations are, respectively, indications of the deterministic and non-deterministic components of variability in the mesoscale anomaly field. In the present context we use deterministic variability to refer the generation or non-generation of an energetic boundary current eddy field as a predictable response to application of time-dependant, external forcing. We use non-deterministic variability to refer to the manifestations of eddy field variability which are not predictable: the number of eddies generated, their individual amplitudes, and locations.

To provide a quantitative measure of the degree of determinism in the numerical simulations of boundary current eddies, monthly energy spectra were computed for the SSH anomaly field along segments of the model eddy corridor in the Alaska Current (130–140°W) and in the Alaskan Stream (155–175°W, cf. Fig. 2). Peak mesoscale wavelengths were identified (218 km for the

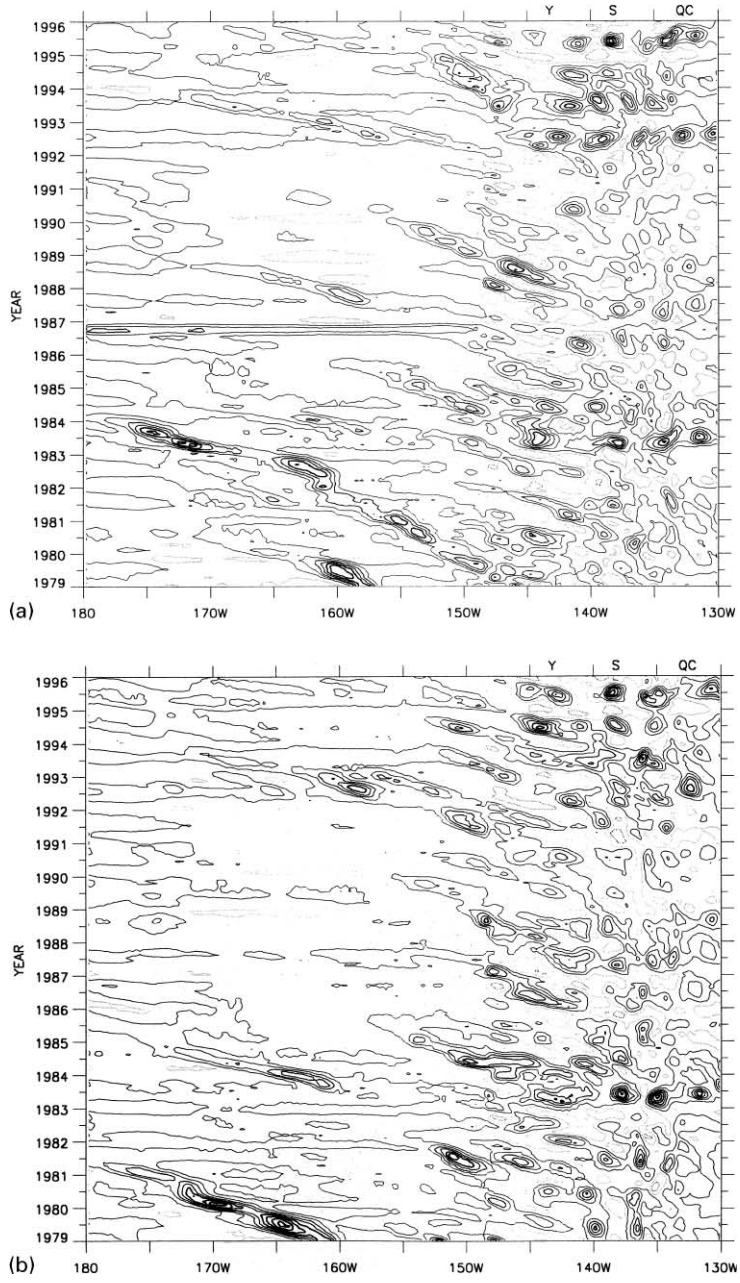

Fig. 7. Time–longitude plots of the SSH anomaly signatures along the eddy corridor for (a) first NLOM simulation, (b) second NLOM simulation. The approximate longitudinal locations of the Yakutat eddy (Y), Sitka eddy (S), and Queen Charlotte eddies (QC) are shown at the top of the figure. Solid line contours indicate zero and positive SSH anomalies and dotted line contours indicate negative SSH anomalies. The contour interval is 5 cm.

Alaska Current segment and 304 km for the Alaskan Stream segment) and the energy spectra for the five Fourier components in the waveband centered on the peak wavelength were averaged and the results plotted as time series (Figs. 8a and b). The reader will note that, because the chosen corridor segments are neither straight nor oriented along meridians or parallels, the distances between adjacent corridor locations vary, and therefore, the derived Fourier wavelengths and

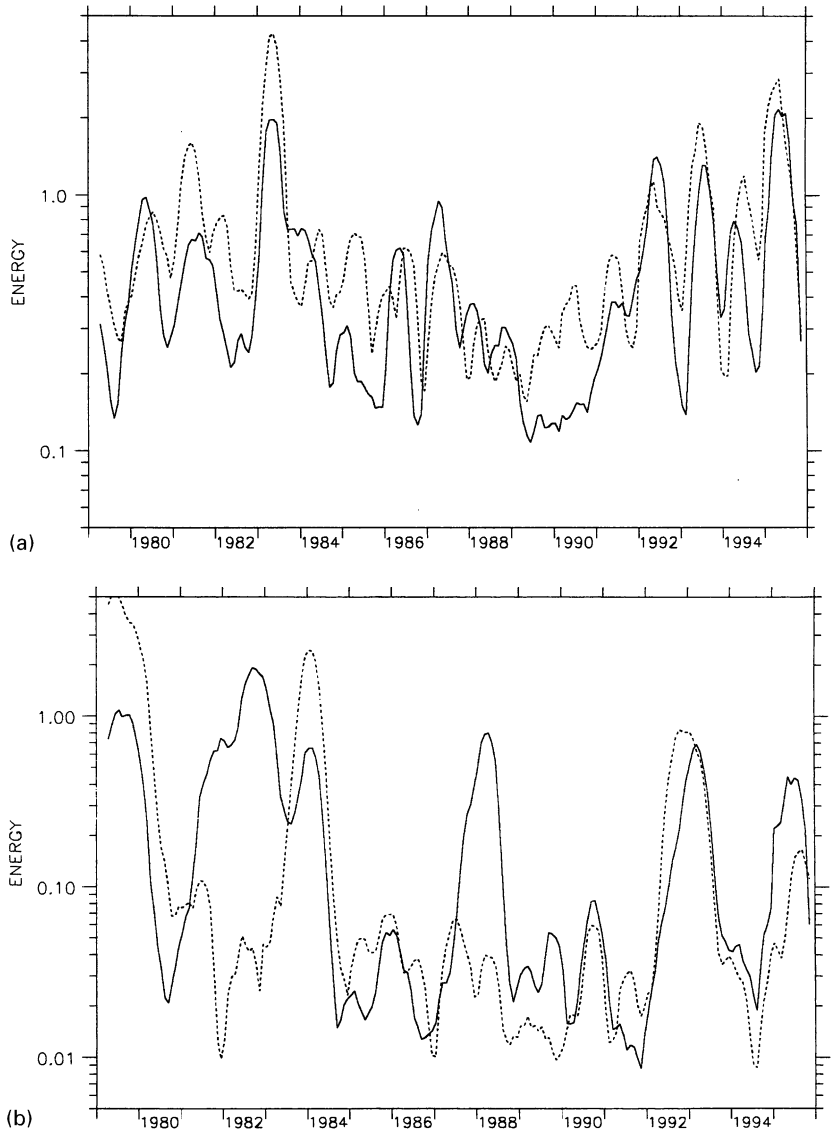

Fig. 8. Time series of averaged spectral energy of model SSH anomalies along the eddy corridor (a) in the Alaska Current and (b) in the Alaskan Stream. Spectral averaging is over the 156–363 km waveband for Alaska Current SSH anomalies and over the 217–506 km waveband for Alaskan Stream SSH anomalies. The solid line and dotted line indicate the average power for the first NLOM simulation and the second NLOM simulation, respectively. A 5-month running mean has been applied to each time series.

their associated spectral energies are approximate. As expected, the companion time series in Figs. 8a and b reflect the similarities and differences of the eddy field simulations illustrated in Figs. 7a and b. It is apparent that there is greater agreement between eddy field simulations in the Alaska Current than in the Alaskan Stream. Correlation coefficients computed for the companion time series (0.65 for the Alaska Current time series and 0.38 for the Alaskan Stream time series) confirm the observation that eddy variability in the Alaska Current is more deterministic than in the Alaskan Stream. The deterministic component of mesoscale variability in the Alaska Current is the focus of the following section.

5. Wind forcing and the generation of eddies in the Alaska Current

From observations and results presented in the previous sections it can be seen that for years in which moderate-to-large amplitude eddies are observed in the altimeter data (Figs. 3–5) and are generated along the BC–Alaska coast by the NLOM (Figs. 7a, b, and 8a) there are corresponding periods during which sea level along the coast is anomalously high (Fig. 6). Reid and Mantyla (1976) observed that for most years during which winter wind forcing over the Gulf of Alaska was strong, coastal sea-level heights were anomalously high. Willmott and Mysak (1980), Tabata (1982), and Swaters and Mysak (1985) all noted a relationship between the strength of the regional wind forcing and the formation of the Sitka eddy. Taken together, these observations suggest that wind forcing is a factor that influences the formation of eddies all along the eastern boundary of the Gulf of Alaska.

A suitable starting point from which to investigate this influence is to consider the sea-level pressure field and associated wind field over the region. Winter (December–February) conditions over the north Pacific Ocean are dominated by the Aleutian low (winter minimum $\sim$1000 mb) whose mean winter position is centered over the Aleutian Islands near 50°N, 170°E and which drives prevailing southwesterly winds into the Gulf of Alaska (Emery and Hamilton, 1985).

Interannual variability with respect to the mean winter conditions was investigated by preparing individual maps of winter sea-level pressure and wind-stress curl fields for each model year. The maps were then compared and considered within the context of the results presented in Figs. 7a, b and 8a. Winter atmospheric conditions for years in which model eddy amplitudes were large (1983) and small (1990) are presented to illustrate the relationship between the regional atmospheric forcing and the associated model eddy field. The 1983 sea-level pressure field (Fig. 9a) shows the Aleutian low to be deeper and centered more than 30° east of its climatological location. In response to the strong pressure gradient in the central and eastern gulf, the associated geostrophic winds exhibit a strong poleward component. Over most of the Gulf of Alaska, the wind-stress curl is positive, whereas orographic interaction with the strong poleward winds creates a region of strong negative curl, extending seaward well beyond the shelfbreak, along the entire eastern boundary of the gulf (Fig. 9b). The 1990 winter sea-level pressure field shows a much weaker Aleutian low and a stronger east Pacific high (Fig. 10a). The more zonal orientation of the isobars results in surface winds having a strong onshore component and a weak along-shore component in the eastern gulf. The coastal mountains steer the onshore wind poleward effecting a zone of positive wind-stress curl all along the coast from the Pacific Northwest to the Alaska

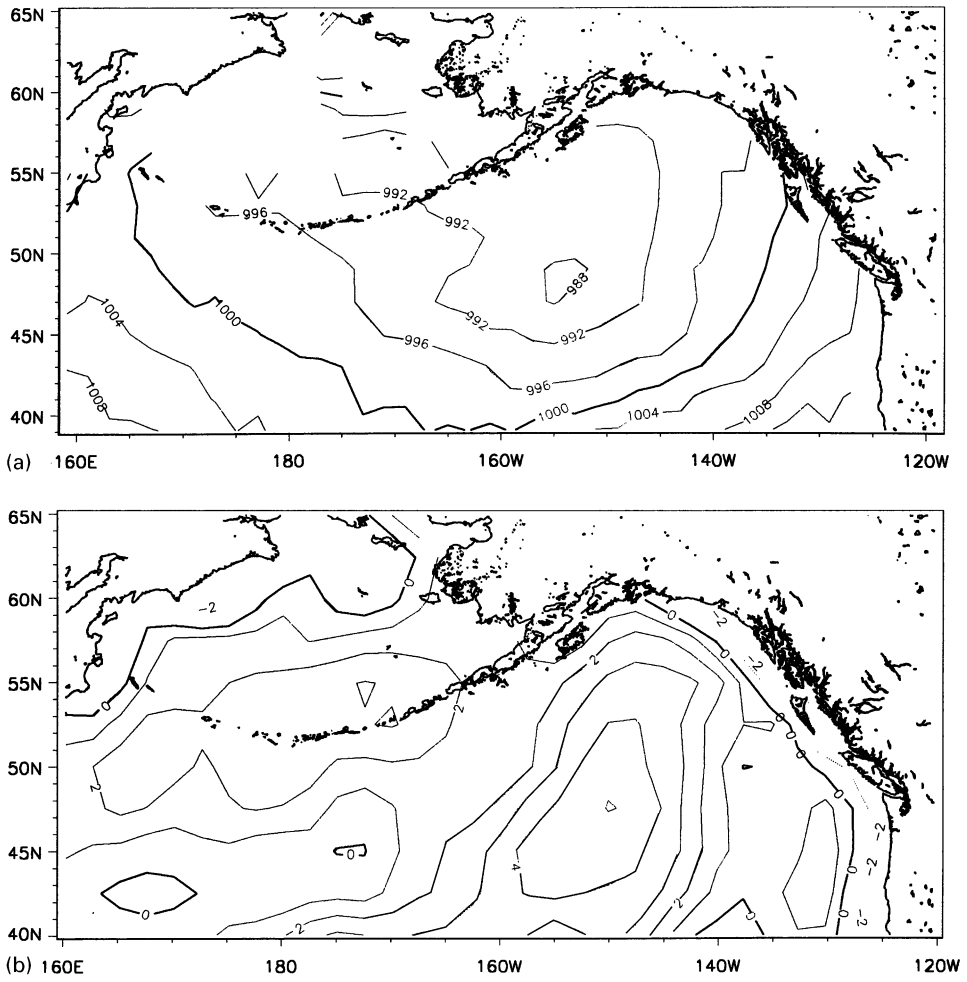

Fig. 9. Mean 1983 winter (December 1982–February 1983) fields of (a) sea-level pressure; the contour interval is 4 mb and (b) wind-stress curl; the contour interval is 1×10^{-7} N m^{-3}.

panhandle (Fig. 10b). Only in the northeast corner of the gulf, over the shelf, is there a small region of negative curl.

In our description of the winter atmospheric conditions over the Gulf of Alaska, we have noted the extent and strength of wind forcing along the BC–Alaska coast. The interannual variability in wind forcing is summarized in time series of non-seasonal wind-stress curl along the BC–Alaska coast (Fig. 11). The interannual variability of wind forcing when compared with the occurrence of NLOM-generated eddies (Fig. 8a) indicates that moderate-to-large amplitude eddies are more likely to form in the Alaska Current during years in which the winter wind-stress curl along the coast and immediately seaward of the shelf break is both anomalously negative and meridionally extensive. This relationship leads us to suggest that Ekman pumping, which is driven by continuity constraints on Ekman transports and in magnitude is proportional to the local wind-stress curl, is a mechanism by which atmospheric forcing can establish conditions in the Alaska

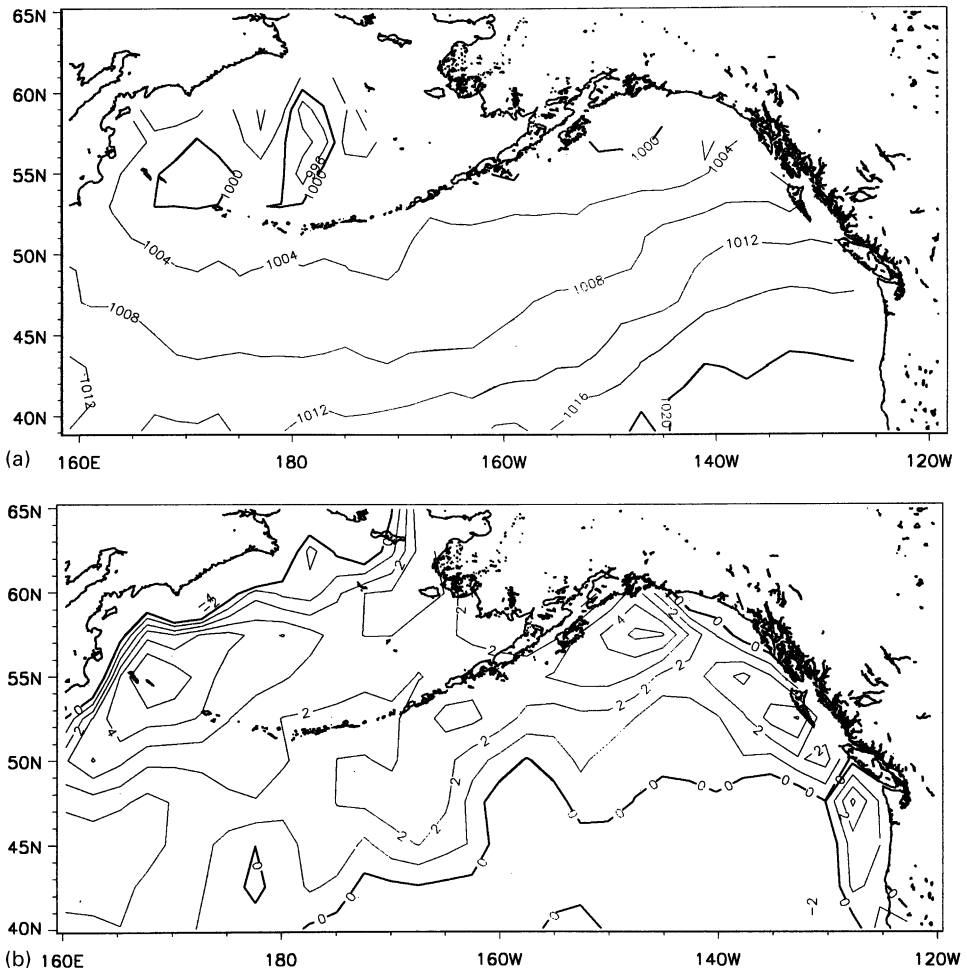

Fig. 10. Same as Fig. 9 except that the fields are for winter 1990.

Current favorable to the generation of eddies. Conceptually, this occurs when strong along-shore winter wind stresses effect Ekman transport of upper layer waters to the BC–Alaska coast where coastal convergence results in downwelling (Ekman pumping). Downwelling locally depresses the pycnocline thereby increasing the onshore declination of the isopycnal surfaces, the result of which is that the Alaska Current becomes increasingly sheared both vertically and horizontally. These shears are necessary for the development of baroclinic and barotropic instabilities from which eddies might evolve. It is not our intent herein to attribute the formation of the eddies in the Alaska Current to either of the instability mechanisms, but rather to indicate that conditions supporting these mechanisms can arise due to Ekman pumping.

The observations presented in this section indicate that moderate-to-large amplitude eddies are generated in the Alaska Current during most years in which wind conditions produce strong downwelling along the eastern boundary of the Alaska gyre. Of these eddies, Yakutat eddies are of particular interest because, of the eddies formed in the Alaska Current, they are the only ones which later propagate into the Alaskan Stream (Figs. 3, 4 and 7). While the altimeter data sets do

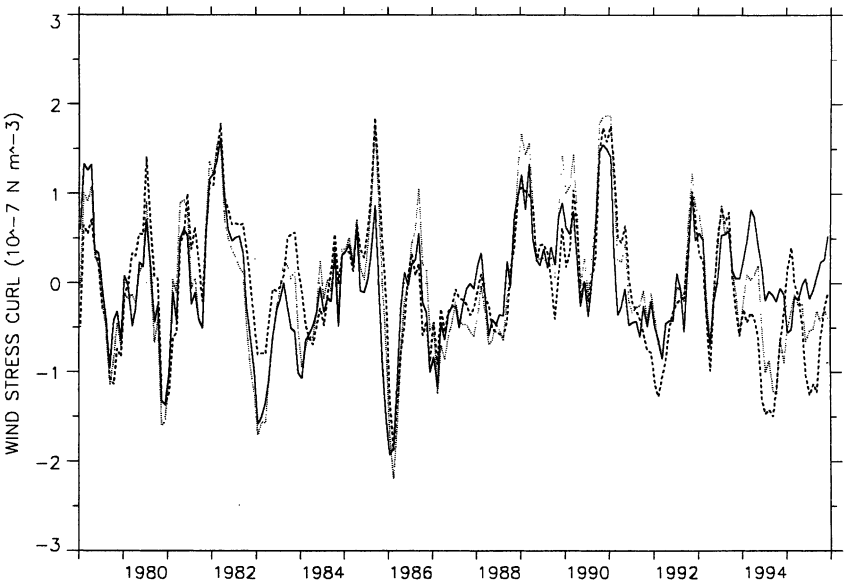

Fig. 11. Time series of the non-seasonal wind-stress curl near the shelf break in the eastern Gulf of Alaska at 50°N, 130°W (dash); 52.5°N, 132.5°W (dot); 55°N, 135°W (solid). A 5-month running mean has been applied to the time series.

not provide sufficient coverage to determine the locations at which eddies A_G, A_T, and B_T were formed, it can be reasonably determined that long-lived, moderate-to-large amplitude, propagating Yakutat eddies were formed in 1987 (C_G), 1992 (C_T), 1994 (D_T), and 1995 (E_T). Additionally, Fig. 3 suggests that eddy B_G is a Yakutat eddy that was formed in 1986. Each of these years is also a year in which the NLOM simulated the formation of a moderate- or large-amplitude Yakutat eddy.

6. Discussion

Observational evidences supported by model results show that, while eddy variability is quite non-deterministic in the Alaskan Stream, moderate-to-large amplitude eddies are formed in the Alaska Current during years in which wind forcing promotes strong downwelling along the BC–Alaska coast. Such wind conditions often, but not always, occur in association with ENSO events. After formation, both observations (e.g. Gower, 1989) and NLOM numerical simulations show that Alaska Current eddies propagate westward away from the eastern boundary so as to delineate the crest of a Rossby-like wave.

The occurrence of Rossby waves in the Gulf of Alaska has been addressed by a number of researchers (e.g. White and Tabata, 1987; Johnson and O'Brien, 1990; Matthews et al., 1992). Those authors all have reported westward phase velocities of roughly $1\,\mathrm{cm\,s^{-1}}$. This value is much faster than is predicted for a linear, non-dispersive Rossby wave ($0.3\,\mathrm{cm\,s^{-1}}$), based upon the 16 km internal deformation radius determined by Emery et al. (1984) to be a representative value for the center of the gyre. Both the observed and modeled eddies comprising the crest of the

Rossby wave have significant amplitudes and longevity which are indicative of non-linearity and resistance to dispersion. These characteristics lead us to speculate that the eddy chain generated along the BC–Alaska coast might be the manifestation of a Rossby soliton. Although the investigation of and search for solitons have generally been limited to the equatorial region (e.g. Boyd, 1980; Kindle, 1983) conditions suitable for the generation and maintenance of solitons occur in the Gulf of Alaska. Boyd (1980) indicates that large amplitude waves, which are excited at boundaries by sudden (impulsive) events, are most likely to generate observable solitons. Flierl (1979) noted that planetary solitary waves (Rossby solitons) are weakly dispersive due to their large size relative to the internal deformation radius, and Redkopp (1977) pointed out that persistent sheared flows are necessary for the existence of solitary Rossby waves.

Another mechanism to which the formation of eddies in the Alaska Current might be attributed is the poleward propagation of Kelvin waves associated with ENSO events. During the period of NLOM simulations, the most significant ENSO events occurred in 1982–1983, 1986–1987, and 1991–1992. Jacobs et al. (1994) showed that a Kelvin wave associated with the 1982–1983 ENSO event triggered a Rossby wave as it moved poleward along the eastern boundary of the Pacific Ocean. The Kelvin wave arrived in the Gulf of Alaska and locally triggered a Rossby wave in 1983. Model results also indicate that Kelvin waves reached the Gulf of Alaska in 1987 and 1992. Because the years in which the ENSO-associated Kelvin waves reach the Gulf of Alaska are also years in which the local wind forcing is strong, it would be difficult to determine the relative influences of wind forcing and Kelvin waves on the formation of Alaska Current eddies.

Uncertainty with respect to the mechanisms influencing the generation and propagation of eddies in the boundary currents of the Alaska gyre remains. The generation of a relatively weak model eddy field and the absence of a significant coastal sea-level rise in 1986, despite strong winter wind forcing, provide evidence for the existence of mechanisms, other than those proposed above, that influence the generation of eddies along the BC–Alaska coast. The large degree of non-deterministic eddy variability in the Alaskan Stream makes an analysis of local deterministic effects difficult. Nonetheless, additional years of observations and numerical simulations should serve to improve understanding of the mechanisms influencing boundary current variability.

The impact of boundary current eddies on the biophysical environment in the Gulf of Alaska is likely significant. It is not unreasonable to expect that region's propagating eddies influence both the exchange of physical properties, nutrients, and biota between the outer shelf and pelagic waters as well as their distribution along the periphery of the Gulf of Alaska.

7. Uncited Reference

Shriver and Hurlburt, 1997.

Acknowledgements

This is a contribution to the following Office of Naval Research sponsored projects: 6.1 Kuroshio Extension Regional Experiment, 6.1 Dynamics of Low Latitude Western Boundary Currents, both program element 601153N, and 6.2 Global Ocean Prediction System, program element 602435N.

The ocean model simulations were performed on the Cray T3E at the Army Corp of Engineers Waterways Experiment Station, Vicksburg, Mississippi and the Cray T3E at the Naval Oceanographic Office, Stennis Space Center, Mississippi under grants of computing time from the Defense Department High Performance Computing Modernization Program. The time on the CEWES Cray T3E was provided under a DOD High Performance Computing Challenge Grant.

References

Boyd, J.P., 1980. Equatorial solitary waves. Part I: Rossby solitons. Journal of Physical Oceanography 10, 1699–1717.

Chelton, D.B., Davis, R.E., 1982. Monthly mean sea-level variability along the west coast of North America. Journal of Physical Oceanography 12, 757–784.

Crawford, W.R., Cherniawsky, J.Y., Foreman, M.G.G., 2000. Multi-year meanders and eddies in the Alaskan Stream as observed by TOPEX/Poseidon altimeter. Geophysical Research Letters 27, 1025–1028.

Cummins, P.F., 1989. A quasi-geostrophic circulation model of the northeast Pacific. Part II: effects of topography and seasonal forcing. Journal of Physical Oceanography 19, 1649–1668.

Cummins, P.F., Mysak, L.A., 1988. A quasi-geosatrophic circulation model of the northeast Pacific. Part I: a preliminary numerical experiment. Journal of Physical Oceanography 18, 1261–1286.

Emery, W.J., Hamilton, K., 1985. Atmospheric forcing of interannual variability in the Northeast Pacific Ocean: connections with El Niño. Journal of Geophysical Research 90, 857–868.

Emery, W.J., Lee, W.G., Magaard, L., 1984. Geographic distributions of density, Brunt-Vaisala frequency and Rossby radii in the North Pacific and North Atlantic. Journal of Physical Oceanography 14, 294–317.

European Centre for Medium-Range Weather Forecasts (ECMWF), 1995. User Guide to ECMWF Products. Meteorological Bulletin M3.2, Reading, England.

Favorite, F., 1974. Flow into the Bering sea through Aleutian Island passes. In: Oceanography of the Bering Sea with Emphasis on Renewable Resources, Vol. 2. Hood, D.W., Kelley, E.J. (Eds.), University of Alaska Occasional Publishers, Fairbanks, Alaska, pp. 3–37.

Flierl, G.R., 1979. Baroclinic solitary waves with radial symmetry. Dynamics of Atmosphere of the Oceans 3, 15–38.

Gibson, J.K., Kallberg, P., Uppala, S., Hernandez, A., Nomura, A., Serrano, E., 1997. ECMWF Re-analysis Project Report Series: 1, ERA Description. ECMWF, Reading, Berkshire, UK, 72pp.

Gower, J.F.R., 1989. Geosat altimeter observations of the distribution and movement of sea-surface height anomalies in the north-east Pacific. In: The Global Ocean, Vol. 3, Oceans '89. IEEE Publication 89CH2780-5, pp. 977–981, Institute of Electronic Engineering, Seattle, Washington.

Hellerman, S., Rosenstein, M., 1983. Normal monthly wind stress over the world ocean with error estimates. Journal of Physical Oceanography 13, 1093–1104.

Hurlburt, H.E., Hogan, P.J., 2000. Impact of 1/8 to 1/64 degree resolution on Gulf Stream model-data comparisons in basin-scale subtropical Atlantic Ocean models. Dyn. Atmos. Ocean. 32, 283–329.

Hurlburt, H.E., Wallcraft, A.J., Schmitz Jr. W.J., Hogan, P.J., Metzger, E.J., 1996. Dynamics of the Kuroshio/Oyashio current system using eddy-resolving models of the North Pacific Ocean. Journal of Geophysical Research 101, 941–976.

Hurlburt, H.E., Metzger, E.J., 1998. Bifurcation of the Kuroshio extension at the Shatsky Rise. Journal of Geophysical Research 103, 7549–7566.

Hurlburt, H.E., Thompson, J.D., 1980. A numerical study of Loop Current intrusions and eddy shedding. Journal of Physical Oceanography 10, 1611–1651.

Jacobs, G.A., Hurlburt, H.E., Kindle, J.C., Metzger, E.J., Mitchell, J.L., Teague, W.J., Wallcraft, A.J., 1994. Decade-scale trans-Pacific propagation and warming effects of an El Niño anomaly. Nature 370, 360–363.

Johnson, M.A., O'Brien, J.J., 1990. The northeast Pacific Ocean response to the 1982–1983 El Niño. Journal of Geophysical Research 95, 7155–7166.

Kindle, J.C., 1983. On the generation of Rossby solitons during El Niño. In: Nihoul, J.C.J. (Ed.), Hydrodynamics of the Equatorial Ocean. Elsevier, Amsterdam, pp. 353–368.

Lagerloef, G.S., Born, G., Leben, R., Royer, T., Musgrave, D., 1993. Mesoscale variations in the Alaska gyre from ERS-1 altimeter data. Second ERS-1 Symposium, Hamburg, 11–14 October.

Lagerloef, G.S., 1995. Interdecadal variations in the Alaska gyre. Journal of Physical Oceanography 25, 2242–2258.

Leben, R.R., Born, G.H., Thompson, J.D., Fox, C.A., 1990. Mean sea surface and variability of the Gulf of Mexico using Geosat altimetry data. Journal of Geophysical Research 95, 3025–3032.

Leonardi, A.P., Hurlburt, H.E., Metzger, E.J., O'Brien, J.J., 2001. Dynamics of the North Hawaiian Ridge Current. J. Phys. Oceanogr., submitted for publication.

Le Provost, C., Genco, M.L., Lyard, F., Vincent, P., Canceil, P., 1994. Spectroscopy of the world ocean tides from a finite element hydrodynamic model. Journal of Geophysical Research 99, 24,777–24,798.

Matthews, P.E., Johnson, M.A., O'Brien, J.J., 1992. Observation of mesoscale ocean features in the northeast Pacific using Geosat radar altimetry data. Journal of Geophysical Research 97, 17,829–17,840.

Melsom, A., Meyers, S.D., Hurlburt, H.E., Metzger, E.J., O'Brien, J.J., 1999. ENSO effects on Gulf of Alaska eddies. Earth Interactions 3(1), 1–1, http://EarthInteractions.org.

Metzger, E.J., Hurlburt, H.E., Kindle, J.C., Rhodes, R.C., Jacobs, G.A., Shriver, J.F., Smedstad, O.M., 1998. The 1997 El Niño in the NRL Layered Ocean Model. 1998 NRL Review, NRL, Washington, DC, pp. 63–71.

Musgrave, D.L., Weingartner, T.J., Royer, T.C., 1992. Circulation and hydrography in the northwestern Gulf of Alaska. Deep-Sea Research 39, 1499–1519.

Mysak, L.A., 1986. El Niño, interannual variability and fisheries in the northeast Pacific Ocean. Canadian Journal of Fisheries and Aquatic Science 43, 464–497.

Okkonen, S.R., 1992. The shedding of an anticyclonic eddy from the Alaskan Stream as observed by the Geosat altimeter. Geophysical Research Letters 19, 2397–2400.

Okkonen, S.R., 1996. The influence of an Alaskan Stream eddy on flow through Amchitka Pass. Journal of Geophysical Research 101, 8839–8851.

Redkopp, L.G., 1977. On the theory of solitary Rossby waves. Journal of Fluid Mechanics 82, 725–745.

Reed, R.K., 1984. Flow of the Alaskan Stream and its variations. Deep-Sea Research 31, 369–386.

Reed, R.K., Muench, R.D., Schumacher, J.D., 1980. On the baroclinic transport of the Alaskan Stream near Kodiak Island. Deep-Sea Research 27, 509–523.

Reed, R.K., Stabeno, P.J., 1989. Recent observations of variability in the path and vertical structure of the Alaskan Stream. Journal of Physical Oceanography 19, 1634–1642.

Reed, R.K., Stabeno, P.J., 1994. Flow along and across the Aleutian Ridge. Journal of Marine Research 52, 639–648.

Reid, J.L., Mantyla, A.W., 1976. The effect of geostrophic flow upon coastal sea elevations in the northern north Pacific Ocean. Journal of Geophysical Research 81, 3100–3110.

Shriver, J.F., Hurlburt, H.E., 1997. The contribution of the global thermohaline circulation to the Pacific to Indian Ocean throughflow via Indonesia. Journal of Geophysical Research 102, 5491–5511.

Shriver, J.F., Hurlburt, H.E., 2000. The effect of upper ocean eddies on the non-steric contribution to the barotropic mode. Geophysics Research Letters 27, 2713–2716.

Swaters, G.E., Mysak, L.A., 1985. Topographically-induced baroclinic eddies near a coastline, with application to the Northeast Pacific. Journal of Physical Oceanography 15, 1470–1485.

Tabata, S., 1982. The anticyclonic, baroclinic eddy off Sitka, Alaska, in the northeast Pacific Ocean. Journal of Physical Oceanography 12, 1260–1282.

Tabata, S., 1991. Annual and interannual variability of baroclinic transports across Line P in the northeast Pacific Ocean. Deep-Sea Research 38, S221–S245.

Thomson, R.E., 1972. On the Alaskan Stream. Journal of Physical Oceanography 2, 363–371.

Thomson, R.E., Gower, J.F.R., 1998. A basin-scale oceanic instability event in the Gulf of Alaska. Journal of Geophysical Research 103, 3033–3040.

Wallcraft, A.J., 1991. The Navy Layered Ocean Model users guide. NOARL Report No. 35, Naval Research Laboratory Stennis Space Center, Mississippi, 21pp.

White, W.B., Tabata, S., 1987. Interannual westward-propagating baroclinic long-wave activity on Line P in the eastern midlatitude North Pacific. Journal of Physical Oceanography 17, 385–396.

Willmott, A.J., Mysak, L.A., 1980. Atmospherically forced eddies in the northeast Pacific. Journal of Physical Oceanography 10, 1769–1791.